INTERNATIONAL JOURNAL FOR NUMERICAL METHODS IN ENGINEERING
Int. J. Numer. Meth. Engng 2005; **64**:1133–1165
Published online 9 May 2005 in Wiley InterScience (www.interscience.wiley.com). DOI: 10.1002/nme.1342

Integration schemes for von-Mises plasticity models based on exponential maps: numerical investigations and theoretical considerations

E. Artioli[1], F. Auricchio[2, 3, *, †] and L. Beirão da Veiga[4]

[1]*D.I.S.T.A.R.T., Universita' di Bologna, Viale del Risorgimento 2, 40136 Bologna, Italy*
[2]*Dipartimento di Meccanica Strutturale, Università di Pavia, Via Ferrata 1, 27100 Pavia, Italy*
[3]*Istituto di Matematica Applicata e Tecnologie Informatiche, CNR, 27100 Pavia, Italy*
[4]*Dipartimento di Matematica 'F. Enriques', Università di Milano, Via Saldini 50, 20133 Milano, Italy*

SUMMARY

We consider three different exponential map algorithms for associative von-Mises plasticity with linear isotropic and kinematic hardening. The first scheme is based on a different formulation of the time continuous plasticity model, which automatically grants the yield consistency of the method in the numerical solution. The second one is the quadratically accurate but non-yield consistent method already proposed in Auricchio and Beirão da Veiga (*Int. J. Numer. Meth. Engng* 2003; **56**: 1375–1396). The third method is an improved version of the second one, in which the yield consistency condition is enforced *a posteriori*. We also compare the performance of the three methods with the classical radial return map algorithm. We develop extensive numerical tests which clearly show the main advantages and disadvantages of the three methods. Copyright © 2005 John Wiley & Sons, Ltd.

KEY WORDS: plasticity; exponential integration algorithm; return map; exact integration; integration factor

1. INTRODUCTION

The present paper is concerned with the development and the numerical evaluation of some exponentially based methods for the associative von-Mises elasto-plastic constitutive model with linear kinematic and isotropic hardening. Expanding an idea of Hong-Ki and Chien-Shan [1], Auricchio and Beirão da Veiga [2] presented a different 'augmented stresses' formulation for this simple but widespread plasticity model. The quasi linearity of the new formulation allowed for an exponential map explicit approximation algorithm for the solution of the system (ENN algorithm). As the authors showed with various numerical tests [2], the derived method

*Correspondence to: F. Auricchio, Dipartimento di Meccanica Strutturale, Università di Pavia, Via Ferrata 1, 27100 Pavia, Italy.
†E-mail: auricchio@unipv.it

Received 2 August 2004
Revised 24 January 2005
Accepted 26 January 2005

amazingly holds quadratic accuracy but it is not consistent with the yield condition, which is a fundamental property in plasticity.

In this paper we propose two different ways to cure this lack of yield consistency. First we introduce a similar but distinct formulation which allows to derive automatically a consistent method (ESC algorithm). Secondly, after a brief review of the ENN algorithm of [2], we introduce a modified version of the ENN which enforces the yield consistency through a radial projection. Then, we develop extensive numerical tests in order to check the accuracy and global convergence properties of the three 'exponential' methods, both on pointwise stress–strain histories and on boundary value problems. The results are also compared with the well established and linearly accurate radial return map method (RRM algorithm), well known also for its great stability properties.

Finally, other interesting algorithmic properties are discussed and compared between the four methods.

Remark 1

Throughout the whole paper we adopt a compact matrix notation. Accordingly, all second rank symmetric tensors are indicated by six components column vectors. The definitions of the trace operator and of the Euclidean norm are consequently modified.

2. TIME CONTINUOUS MODEL

We consider an associative von-Mises plasticity model with linear kinematic and isotropic hardening in the realm of small deformations (refer for example to Reference [3] or [4]). Accordingly, the volumetric plastic strain is zero, leading to a deviatoric-volumetric decoupling, and therefore it is convenient to split the strain and stress vectors, $\boldsymbol{\sigma}$ and $\boldsymbol{\varepsilon}$, as

$$\boldsymbol{\sigma} = \mathbf{s} + p\mathbf{i} \text{ with } \quad p = \tfrac{1}{3}\mathrm{tr}(\boldsymbol{\sigma}) \tag{1}$$

$$\boldsymbol{\varepsilon} = \mathbf{e} + \tfrac{1}{3}\theta\mathbf{i} \text{ with } \quad \theta = \mathrm{tr}(\boldsymbol{\varepsilon}) \tag{2}$$

where tr indicates the trace operator (sum of the first three components), while $\mathbf{i}, \mathbf{s}, p, \mathbf{e}, \theta$ are, respectively, the vector corresponding to the second rank identity tensor, the deviatoric and volumetric stresses, the deviatoric and volumetric strains.

Accordingly, the equations for the model are

$$p = K\theta \tag{3}$$

$$\mathbf{s} = 2G[\mathbf{e} - \mathbf{e}^{\mathrm{p}}] \tag{4}$$

$$\boldsymbol{\Sigma} = \mathbf{s} - \boldsymbol{\alpha} \tag{5}$$

$$F = \|\boldsymbol{\Sigma}\| - \sigma_{\mathrm{y}} \tag{6}$$

$$\dot{\mathbf{e}}^{\mathrm{p}} = \dot{\gamma}\mathbf{n} \tag{7}$$

$$\sigma_{\mathrm{y}} = \sigma_{\mathrm{y},0} + H_{\mathrm{iso}}\gamma \tag{8}$$

$$\dot{\boldsymbol{\alpha}} = H_{\text{kin}}\dot{\mathbf{e}}^{\text{p}} \tag{9}$$

$$\dot{\gamma} \geqslant 0, \quad F \leqslant 0, \quad \dot{\gamma}F = 0 \tag{10}$$

where

- Equation (3) represents the volumetric elastic relation, with K the material bulk modulus.
- Equation (4) represents the deviatoric elastic relation, with G the material shear modulus, $\mathbf{e}^{\text{p}}$ the traceless plastic strain, and where we use the standard additive strain decomposition $\mathbf{e} = \mathbf{e}^{\text{e}} + \mathbf{e}^{\text{p}}$.
- Equation (5) expresses the relative stress $\boldsymbol{\Sigma}$ in terms of the backstress $\boldsymbol{\alpha}$, introduced to describe a kinematic hardening mechanism.
- Equation (6) is the von Mises yield function, expressed in terms of the relative stress $\boldsymbol{\Sigma}$, where $\| \bullet \|$ is the Euclidean norm and σ_{y} the yield stress.
- Equation (7) determines the evolution of the plastic strain, where γ is a scalar quantity known as consistency parameter, the superposed dot indicates a time derivative, while $\mathbf{n}$ is defined as

$$\mathbf{n} = \frac{\partial F}{\partial \boldsymbol{\Sigma}} = \frac{\boldsymbol{\Sigma}}{\| \boldsymbol{\Sigma} \|} \tag{11}$$

- Equation (8) represents a linear isotropic hardening mechanism, governing the radius of the yield surface $F = 0$. In particular $\sigma_{\text{y},0}$ is the initial yield stress and H_{iso} is a material constant.
- Equation (9) represents a linear kinematic hardening mechanism, governing the evolution of the backstress $\boldsymbol{\alpha}$, hence the shift of the yield function in the stress space. The scalar H_{kin} is a material constant.
- Equations (10) are the Kuhn–Tucker conditions. In particular, the second equation limit the relative stress within the boundary defined by the yield surface $F = 0$, while the other two are necessary to determine the plastic strain behaviour. With a slight over-simplification of the model complexity, we may say that when $\dot{\gamma} = 0$ the system is in an elastic phase, while when $\dot{\gamma} > 0$ we say that the system is in a plastic phase.

Remark 2
We observe that, due to its simple linear behaviour, finding the exact solution of the volumetric part is immediate; therefore, in the sequel we treat only the more interesting deviatoric part of the model.

3. RADIAL RETURN MAP

We now briefly review a classical numerical method used to approach the solution of the described plasticity model, the radial return map, for which a more detailed description can be found in several articles and books [5–8]. In general, the method consists in:

1. the time-integration of the differential algebraic system (4)–(10), leading to an algebraic system;
2. the formulation of a solution algorithm for the obtained algebraic system.

As an example, the time-integration procedure may be obtained using a first-order backward Euler formula; accordingly, the algebraic system solution reduces to a radial return map. In the following we quickly recall the method together with the form of the consistent tangent.

Solution algorithm: Assuming that the time history interval $[0, T]$ is divided into N sub-intervals defined by the points $0 = t_0 < t_1 < \cdots < t_n < t_{n+1} < \cdots < t_N = T$, given the values $(\mathbf{s}_n, \mathbf{e}_n, \gamma_n, \boldsymbol{\alpha}_n)$ at time t_n, and the deviatoric strain $\mathbf{e}_{n+1}$ at time t_{n+1}, we search for the remaining variables at time t_{n+1}. Note that in the construction of the algorithm the strain history is implicitly assumed to be piecewise linear.

We initially suppose the step to be elastic, and calculate trial values

$$\begin{aligned} \mathbf{e}_{n+1}^{\mathrm{p,TR}} &= \mathbf{e}_n^{\mathrm{p}} \\ \mathbf{s}_{n+1}^{\mathrm{TR}} &= 2G[\mathbf{e}_{n+1} - \mathbf{e}_n^{\mathrm{p}}] \\ \boldsymbol{\alpha}_{n+1}^{\mathrm{TR}} &= \boldsymbol{\alpha}_n \\ \boldsymbol{\Sigma}_{n+1}^{\mathrm{TR}} &= \mathbf{s}_{n+1}^{\mathrm{TR}} - \boldsymbol{\alpha}_{n+1}^{\mathrm{TR}} \\ \gamma_{n+1}^{\mathrm{TR}} &= \gamma_n \end{aligned} \tag{12}$$

If the resulting stress is admissible, i.e.

$$\| \boldsymbol{\Sigma}_{n+1}^{\mathrm{TR}} \| \leqslant \sigma_{\mathrm{y},0} + H_{\mathrm{iso}} \gamma_{n+1}^{\mathrm{TR}} \tag{13}$$

the variable values at the time instant t_{n+1} are taken as the trial ones just calculated. On the other hand, if $\boldsymbol{\Sigma}_{n+1}^{\mathrm{TR}}$ violates the yield limit (13), a plastic correction is introduced

$$\begin{aligned} \mathbf{e}_{n+1}^{\mathrm{p}} &= \mathbf{e}_{n+1}^{\mathrm{p,TR}} + \lambda \mathbf{n} \\ \mathbf{s}_{n+1} &= \mathbf{s}_{n+1}^{\mathrm{TR}} - 2G\lambda \mathbf{n} \\ \boldsymbol{\alpha}_{n+1} &= \boldsymbol{\alpha}_{n+1}^{\mathrm{TR}} + H_{\mathrm{kin}} \lambda \mathbf{n} \\ \boldsymbol{\Sigma}_{n+1} &= \boldsymbol{\Sigma}_{n+1}^{\mathrm{TR}} - [2G + H_{\mathrm{kin}}]\, \lambda \mathbf{n} \\ \gamma_{n+1} &= \gamma_{n+1}^{\mathrm{TR}} + \lambda \end{aligned} \tag{14}$$

where the scalar λ represents the increment of the plastic consistency parameter, i.e.

$$\lambda = \int_{t_n}^{t_{n+1}} \dot{\gamma}\, \mathrm{d}t \tag{15}$$

The solution of the algebraic system (14) is approached solving initially for the scalar λ, enforcing the condition $F(\boldsymbol{\Sigma}_{n+1}) = 0$. This implicit equation is solved observing that $\boldsymbol{\Sigma}_{n+1}^{\mathrm{TR}}$ and $\boldsymbol{\Sigma}_{n+1}$ are parallel, in other words

$$\mathbf{n} = \frac{\boldsymbol{\Sigma}_{n+1}}{\| \boldsymbol{\Sigma}_{n+1} \|} = \frac{\boldsymbol{\Sigma}_{n+1}^{\mathrm{TR}}}{\| \boldsymbol{\Sigma}_{n+1}^{\mathrm{TR}} \|} = \mathbf{n}^{\mathrm{TR}} \tag{16}$$

obtaining

$$\lambda = \frac{\| \boldsymbol{\Sigma}_{n+1}^{\mathrm{TR}} \| - \left(\sigma_{\mathrm{y},0} + H_{\mathrm{iso}} \gamma_{n+1}^{\mathrm{TR}}\right)}{2G + H_{\mathrm{iso}} + H_{\mathrm{kin}}} \tag{17}$$

Once the scalar λ is known, taking advantage of (16), it is possible to update all the problem variables following (14).

Tangent matrix: The algorithmically consistent tangent matrix is obtained linearizing the time-discrete algorithmic procedure. In particular, for a plastic step (i.e. $\lambda \neq 0$), we get

$$\mathbb{D}_{\mathrm{disc}} = K(\mathbf{i}\,\mathbf{i}^{\mathrm{T}}) + 2G(1-C)\mathbb{I}_{\mathrm{dev}} + [2G(C-A)]\mathbf{n}^{\mathrm{TR}}[\mathbf{n}^{\mathrm{TR}}]^{\mathrm{T}} \tag{18}$$

where the superscript T indicates the transpose and

$$A = \frac{2G}{2G + H_{\mathrm{iso}} + H_{\mathrm{kin}}} \tag{19}$$

$$C = \frac{2G\lambda}{\| \boldsymbol{\Sigma}_{n+1}^{\mathrm{TR}} \|} \tag{20}$$

$$\mathbb{I}_{\mathrm{dev}} = \mathbb{I} - \tfrac{1}{3}\,\mathbf{i}\,\mathbf{i}^{\mathrm{T}} \tag{21}$$

$\mathbb{I}$ being the identity matrix. The calculation of $\mathbb{D}_{\mathrm{disc}}$ hides no particular difficulties and details can be found for example in Reference [7].

4. A NEW MODEL FORMULATION

Before addressing the new integration schemes, we need to convert the original differential problem in a different but equivalent one. In fact, as noted in the literature [1, 2, 9], an associative von-Mises plasticity model with linear kinematic hardening can be formulated as a differential problem of the following type:

$$\dot{\mathbf{X}} = \mathbb{A}\mathbf{X} \tag{22}$$

where the matrix $\mathbb{A}$ may depend on $\mathbf{X}$.

Accordingly, the goal of the present section is to propose a new model re-formulation in format (22), which is an improved (symmetric) version of the one proposed in Reference [2]. Afterwards, we derive a numerical scheme to solve our dynamical system (22).

Formulation (22) is obtained as follows. The Combination of Equations (4) and (5) leads to

$$\boldsymbol{\Sigma} + \boldsymbol{\alpha} + 2G\mathbf{e}^{\mathrm{p}} = 2G\mathbf{e} \tag{23}$$

which, taking the derivative in time, applying Equation (9) and rearranging terms gives

$$\dot{\boldsymbol{\Sigma}} = 2G\dot{\mathbf{e}} - (2G + H_{\mathrm{kin}})\dot{\mathbf{e}}^{\mathrm{p}} \tag{24}$$

Now, introducing the yield surface radius

$$R := \sigma_{\mathrm{y},0} + H_{\mathrm{iso}}\gamma \tag{25}$$

and recalling that in the plastic phase

$$\mathbf{n} = \frac{\boldsymbol{\Sigma}}{\|\boldsymbol{\Sigma}\|} = \frac{\boldsymbol{\Sigma}}{\sigma_{y,0} + H_{\text{iso}}\gamma} = \frac{\boldsymbol{\Sigma}}{R} \tag{26}$$

we may apply (7) obtaining

$$\dot{\boldsymbol{\Sigma}} + (2G + H_{\text{kin}}) \frac{\boldsymbol{\Sigma}}{R} \dot{\gamma} = 2G\dot{\mathbf{e}} \tag{27}$$

which is a differential equation for $\boldsymbol{\Sigma}$. Note that the above equation is valid also during elastic phases ($\dot{\gamma} = 0$). We now introduce the *scaled relative stress*

$$\bar{\boldsymbol{\Sigma}} := \frac{\boldsymbol{\Sigma}}{R} \tag{28}$$

and observe that, whenever the relative stress $\boldsymbol{\Sigma}$ lays on the yield surface, then $\bar{\boldsymbol{\Sigma}} = \mathbf{n}$, while this is not true when $\boldsymbol{\Sigma}$ lays inside the yield surface. Taking the time derivative of (28) and recalling (25) gives

$$\dot{\bar{\boldsymbol{\Sigma}}} = \frac{\dot{\boldsymbol{\Sigma}}}{R} - \frac{H_{\text{iso}}}{R} \dot{\gamma}\bar{\boldsymbol{\Sigma}} \tag{29}$$

Dividing Equation (27) by R and using relationship (29), one obtains

$$\dot{\bar{\boldsymbol{\Sigma}}} + \frac{2G + H_{\text{kin}} + H_{\text{iso}}}{R} \dot{\gamma}\bar{\boldsymbol{\Sigma}} = \frac{2G}{R} \dot{\mathbf{e}} \tag{30}$$

The next goal is to introduce an integrating factor. Accordingly, we set

$$X_0(\gamma) = \begin{cases} \left(1 + \dfrac{H_{\text{iso}}}{\sigma_{y,0}}\gamma\right)^{\frac{2G+H_{\text{kin}}+H_{\text{iso}}}{H_{\text{iso}}}} & \text{if } H_{\text{iso}} \neq 0 \\ \exp\left(\dfrac{2G + H_{\text{kin}} + H_{\text{iso}}}{\sigma_{y,0}}\gamma\right) & \text{if } H_{\text{iso}} = 0 \end{cases} \tag{31}$$

noting that such a function is continuous for fixed γ and $H_{\text{iso}} \to 0$, and that

$$\dot{X}_0 = \frac{2G + H_{\text{kin}} + H_{\text{iso}}}{R} \dot{\gamma} X_0 \tag{32}$$

It is evident that multiplying Equation (30) by X_0 and using Equation (32) the following relationship holds:

$$\frac{\mathrm{d}}{\mathrm{d}t}[X_0\bar{\boldsymbol{\Sigma}}] = X_0\dot{\bar{\boldsymbol{\Sigma}}} + \dot{X}_0\bar{\boldsymbol{\Sigma}} = \frac{2G}{R} X_0\dot{\mathbf{e}} \tag{33}$$

At this stage, defining a new 7-dimensional *generalized stress vector* $\mathbf{X}$ as

$$\mathbf{X} = \begin{pmatrix} X_0\bar{\boldsymbol{\Sigma}} \\ X_0 \end{pmatrix} = \begin{pmatrix} \mathbf{X}^{\text{s}} \\ X_0 \end{pmatrix} \tag{34}$$

Equation (33) can be rewritten as

$$\dot{\mathbf{X}}^{\mathrm{s}} = \frac{2G}{R} X_0 \dot{\mathbf{e}} \tag{35}$$

Now as last step to obtain system (22), we need an evolution law for X_0 in terms of $\mathbf{X}$, which in elastic phases follows immediately from (32):

$$\dot{X}_0 = 0 \quad \text{(elastic phases)} \tag{36}$$

On the other hand, for $\dot{\gamma} \neq 0$, we take the scalar product of (33) with $\bar{\mathbf{\Sigma}}$, obtaining

$$X_0 \frac{1}{2} \frac{\mathrm{d}}{\mathrm{d}t} \| \bar{\mathbf{\Sigma}} \|^2 + \dot{X}_0 \| \bar{\mathbf{\Sigma}} \|^2 = \frac{2G}{R} X_0 \dot{\mathbf{e}}^{\mathrm{T}} \bar{\mathbf{\Sigma}} \tag{37}$$

Therefore, noting that in plastic phases

$$\| \bar{\mathbf{\Sigma}} \| = \frac{\| \mathbf{\Sigma} \|}{R} = 1 \tag{38}$$

and using (34) as well as (37), we easily get

$$\dot{X}_0 = \frac{2G}{R} \dot{\mathbf{e}}^{\mathrm{T}} \mathbf{X}^{\mathrm{s}} \quad \text{(plastic phases)} \tag{39}$$

Consequently, Equations (35) and (36)–(39) provide a system for the generalized stress vector $\mathbf{X}$ in the form

$$\dot{\mathbf{X}} = \mathbb{A}\mathbf{X} \tag{40}$$

with the matrix $\mathbb{A}$ depending on the actual phase as follows

$$\mathbb{A} = \frac{2G}{R} \begin{pmatrix} \mathbf{0}_{6\times 6} & \dot{\mathbf{e}} \\ \mathbf{0}_{1\times 6} & 0 \end{pmatrix} \quad \text{(elastic phase)} \tag{41}$$

$$\mathbb{A} = \frac{2G}{R} \begin{pmatrix} \mathbf{0}_{6\times 6} & \dot{\mathbf{e}} \\ \dot{\mathbf{e}}^{\mathrm{T}} & 0 \end{pmatrix} \quad \text{(plastic phase)} \tag{42}$$

Therefore, the original problem, expressed by Equations (4)–(9), has been substituted by a new one, expressed by Equations (40)–(42).

We must note that in the case of no isotropic hardening ($H_{\mathrm{iso}} = 0$) the radius is fixed, and therefore $\mathbb{A}$ depends only on $\dot{\mathbf{e}}$. This means that, if $\dot{\mathbf{e}}$ is constant in a certain time interval, $\mathbb{A}$ holds the same property: under such a hypothesis the solution of system (40) is known and the problem can be solved exactly.

However, in a general case ($H_{\mathrm{iso}} \neq 0$) the matrix $\mathbb{A}$ depends on $\mathbf{X}$, and in this sense we say that the problem is quasi linear. Anyway, the partial linearity arising in the problem is indeed of great value, allowing us to develop the numerical method of Section 5.

4.1. Time-continuous on–off switch

To properly convert the original problem in an equivalent but new differential algebraic format, we also need to introduce an elasto-plastic phase determination criteria expressed in the new generalized stress environment.

For a given state to be plastic, the following two conditions must be fulfilled:

(1) The relative stress $\boldsymbol{\Sigma}$ must be on the yield surface, in other words

$$\| \boldsymbol{\Sigma} \| = R \tag{43}$$

Using (28) and (34) this can be easily rewritten as

$$\| \mathbf{X}^{\mathrm{s}} \|^2 = \| \bar{\boldsymbol{\Sigma}} \|^2 \, X_0^2 = \frac{\| \boldsymbol{\Sigma} \|^2}{R^2} \, X_0^2 = X_0^2 \tag{44}$$

(2) The direction of the strain rate $\dot{\mathbf{e}}$ must be outward with respect to the yield surface, i.e.

$$\boldsymbol{\Sigma}^{\mathrm{T}} \dot{\mathbf{e}} > 0 \tag{45}$$

Again recalling (28) and (34) it is immediate to check that (45) is equivalent to

$$(\mathbf{X}^{\mathrm{s}})^{\mathrm{T}} \dot{\mathbf{e}} > 0 \tag{46}$$

If either one of the two conditions (44) and (46) is not satisfied then, the phase is elastic.

5. NUMERICAL ALGORITHM

We now want to develop a numerical scheme for the evolution of $\mathbf{X}$, governed by the dynamical law (40) with matrix $\mathbb{A}$ given by (41) and (42). For simplicity, we consider the initial values of $\gamma, \mathbf{e}^{\mathrm{p}}$ and $\boldsymbol{\alpha}$ to be zero, so that the initial generalized stress vector is

$$\mathbf{X}_0 = \begin{pmatrix} \boldsymbol{\Sigma}_0 / R_0 \\ 1 \end{pmatrix} \tag{47}$$

As usual, we assume that the time history interval $[0, T]$ is divided into N sub-intervals defined by the points $0 = t_0 < t_1 < \cdots < t_n < t_{n+1} < \cdots < t_N = T$, given the values $(\mathbf{s}_n, \mathbf{e}_n, \gamma_n, \boldsymbol{\alpha}_n)$ at time t_n, and the deviatoric strain $\mathbf{e}_{n+1}$ at time t_{n+1} and we search for the remaining variables at time t_{n+1}. Note that also in the construction of this algorithm the strain history is assumed to be piecewise linear.

Due to the piecewise linearity of the strain path, $\dot{\mathbf{e}}$ is constant in each single time interval. Unluckily, due to the presence of R in (42), this is not true for matrix $\mathbb{A}$; the yield surface radius R is a function of X_0, and so of $\mathbf{X}$, as shown by relation (32). Therefore, we approximate the solution of dynamical law (40) considering $R = R_n$ constant in each single time step (with R_n the value at the beginning of the step). Under such an additional hypothesis, the matrix $\mathbb{A}$ is constant in both phases and Equation (40) can be solved exactly, giving the following evolution for $\mathbf{X}$:

$$\mathbf{X}_{n+1} = \exp\left[\mathbb{A}_n \Delta t\right] \mathbf{X}_n = \bar{\mathbb{G}} \mathbf{X}_n \tag{48}$$

where $\Delta t = t_{n+1} - t_n$. Defining the vector $\Delta\mathbf{e} = \mathbf{e}_{n+1} - \mathbf{e}_n$, we observe that the matrix $\mathbb{A}_n \Delta t$ is equal to the matrix (41) or (42) after substituting $\dot{\mathbf{e}}$ with $\Delta\mathbf{e}$. Therefore, the matrix $\bar{\mathbb{G}}$ is

$$\bar{\mathbb{G}} = \begin{cases} \bar{\mathbb{G}}_{\mathrm{e}} = \begin{pmatrix} \mathbb{I} & \dfrac{2G}{R_n}\Delta\mathbf{e} \\ 0 & 1 \end{pmatrix} & \text{(elastic phase)} \\ \bar{\mathbb{G}}_{\mathrm{p}} = \begin{pmatrix} \mathbb{I} + \left[\dfrac{(a-1)}{\|\Delta\mathbf{e}\|^2}\right]\Delta\mathbf{e}\Delta\mathbf{e}^{\mathrm{T}} & b\,\dfrac{\Delta\mathbf{e}}{\|\Delta\mathbf{e}\|} \\ b\,\dfrac{\Delta\mathbf{e}^{\mathrm{T}}}{\|\Delta\mathbf{e}\|} & a \end{pmatrix} & \text{(plastic phase)} \end{cases} \tag{49}$$

where the scalars a and b are

$$a = \cosh\left(\frac{2G}{R_n}\ \|\Delta\mathbf{e}\|\right) \tag{50}$$

$$b = \sinh\left(\frac{2G}{R_n}\ \|\Delta\mathbf{e}\|\right) \tag{51}$$

In conclusion, at every time step the numerical scheme is as follows:

(1) Suppose the step to be elastic and compute trial values following an elastic law:

$$\mathbf{X}_{n+1}^{\mathrm{TR}} = \bar{\mathbb{G}}_{\mathrm{e}}\mathbf{X}_n \tag{52}$$

where the matrix $\bar{\mathbb{G}}_{\mathrm{e}}$ is given by (49). If the trail solution is admissible, i.e.

$$\|\mathbf{X}_{n+1}^{\mathrm{s,TR}}\| \leqslant (X_{0,n+1}^{\mathrm{TR}})^2 \tag{53}$$

then the variable values at the time step t_{n+1} are taken as the trial ones just calculated.

(2) If the trial solution is non-admissible, i.e. Equation (53) is violated, then the step is plastic. Being $\dot{\mathbf{e}}$ constant in each time sub interval, this means that the step can be divided into two parts: an elastic deformation followed by a plastic one. We represent with a scalar $\alpha \in [0, 1)$ the elastic time proportion of the step; for example $\alpha = \frac{1}{2}$ means that the stress evolution is of elastic kind for the first half of the time interval, and plastic in the rest. Note that $\alpha = 1$ is not admissible since it would imply a complete elastic step, which is not possible at this stage since we have admitted the step to be plastic. Simple geometrical considerations allow us to compute α; omitting the details, we obtain

$$\alpha = \frac{\sqrt{C^2 - DM} - C}{D} \tag{54}$$

where

$$\begin{cases} C = \dfrac{2GX_{0,n}}{R_n}(\mathbf{X}_n^{\mathrm{s}})^{\mathrm{T}}\Delta\mathbf{e} \\ D = \left(\dfrac{2GX_{0,n}\ \|\Delta\mathbf{e}\|}{R_n}\right)^2 \\ M = \|\mathbf{X}_n^{\mathrm{s}}\|^2 - (X_{0,n+1}^{\mathrm{TR}})^2 \end{cases} \tag{55}$$

Computed α, $\mathbf{X}_{n+1}$ is updated in two steps.

– Calculate a new $\mathbf{X}_{n+1}^{\mathrm{TR}}$ following an elastic law

$$\mathbf{X}_{n+1}^{\mathrm{TR}} = \bar{\mathbb{G}}_{\mathrm{e}} \mathbf{X}_n \tag{56}$$

with $\bar{\mathbb{G}}_{\mathrm{e}}$ still given by (49), but where $\Delta\mathbf{e} = \alpha(\mathbf{e}_{n+1} - \mathbf{e}_n)$ instead of $\Delta\mathbf{e} = (\mathbf{e}_{n+1} - \mathbf{e}_n)$.
– Calculate $\mathbf{X}_{n+1}$ evolving from the new initial data $\mathbf{X}_{n+1}^{\mathrm{TR}}$ following a plastic law

$$\mathbf{X}_{n+1} = \bar{\mathbb{G}}_{\mathrm{p}} \mathbf{X}_{n+1}^{\mathrm{TR}} \tag{57}$$

with $\bar{\mathbb{G}}_{\mathrm{p}}$ given by (49), where $\Delta\mathbf{e} = (1-\alpha)(\mathbf{e}_{n+1} - \mathbf{e}_n)$ instead of $\Delta\mathbf{e} = (\mathbf{e}_{n+1} - \mathbf{e}_n)$.

Observe that in such a framework purely plastic steps are simply those where the time proportion of elastic phase α is zero.

(3) Finally at the end of each step update the yield surface radius

$$R_{n+1} = R(X_{0,\,n+1}) = \sigma_{\mathrm{y},\,0}(X_{0,\,n+1})^{\frac{H_{\mathrm{iso}}}{2G+H_{\mathrm{kin}}+H_{\mathrm{iso}}}} \tag{58}$$

which is easily obtained combining (25) and (31).

Note that the relative stress and backstress can be calculated whenever needed as

$$\boldsymbol{\Sigma} = \frac{\mathbf{X}^{\mathrm{s}}}{X_0} R \tag{59}$$

$$\boldsymbol{\alpha} = H_{\mathrm{kin}} \frac{2G\mathbf{e} - \boldsymbol{\Sigma}}{2G + H_{\mathrm{kin}}} \tag{60}$$

The first one is immediately obtained from the definition of $\mathbf{X}$, while the second one follows from (4) and (5), observing that $\boldsymbol{\alpha} = H_{\mathrm{kin}} \mathbf{e}^{\mathrm{p}}$.

Remark 3
The numerical scheme proposed in this section is fully consistent with the yield surface condition. In other words, during each plastic step condition (44) holds also for the numerical solution, differently from the scheme proposed in Reference [2] (and briefly recalled in Section (6)). The proof of this is quite easy and is addressed in the Appendix.

Remark 4
We observe that, dividing the augmented stressed $\mathbf{X}$ by any positive scalar does not lead to any change in the output vector $\boldsymbol{\Sigma}$ (see (59)) because both $\mathbf{X}^{\mathrm{s}}$ and X_0 are divided by the same amount. This leads to the two following observations when the algorithm is implemented.

- The scalar X_0 does not need to be dynamically updated. Therefore it is not an history variable; instead, it is used as an auxiliary variable and can be conventionally set equal to 1 at the start of each time step. Note that this is equivalent to scaling the $\mathbf{X}$ vector by X_0 at the beginning of each time step. The history variables which need to be updated step by step are $\boldsymbol{\Sigma}$ and R.
- Due to the consideration above, the matrix $\mathbb{G}_{\mathrm{p}}$ can be divided by any positive scalar without changing the final output. Therefore, scaling $\mathbb{G}_{\mathrm{p}}$ by $\cosh[(2G/R_n) \| \Delta\mathbf{e} \|)]$ avoids risks of overflow errors when the ratio $(2G/R_n) \| \Delta\mathbf{e} \|$ is large (see (49)). This point is

particularly important when the algorithm is inserted in a global finite element problem; this is why the authors avoided a 'Cayley transform' approximation of system (40), proposed in Reference [10] (see Section 7.3 for more details).

5.1. Tangent matrix

The algorithmically consistent tangent matrix can be obtained properly linearizing the time-discrete procedure. In the present paragraph all dynamical discrete quantities are evaluated at the end of the actual time step t_{n+1}; therefore all subscripts will be omitted for the sake of compactness. From the definition of the generalized stress vector $\mathbf{X}$ we get

$$\frac{\partial \mathbf{X}^{\mathrm{s}}}{\partial \mathbf{e}} = \frac{X_0}{R}\frac{\partial \boldsymbol{\Sigma}}{\partial \mathbf{e}} + \frac{\boldsymbol{\Sigma}}{R}\frac{\partial X_0}{\partial \mathbf{e}} + X_0\boldsymbol{\Sigma}\frac{\partial}{\partial \mathbf{e}}\left(\frac{1}{R}\right) \tag{61}$$

Introducing

$$\beta = \frac{H_{\mathrm{iso}}}{2G + H_{\mathrm{iso}} + H_{\mathrm{kin}}} \tag{62}$$

and recalling (58), a direct derivation gives

$$\frac{\partial}{\partial \mathbf{e}}\left(\frac{1}{R}\right) = \frac{1}{\sigma_{\mathrm{y},0}}\frac{\partial}{\partial \mathbf{e}}X_0^{-\beta} = -\beta\frac{1}{X_0 R}\frac{\partial X_0}{\partial \mathbf{e}} \tag{63}$$

From (61) and (63), using also definition (34) it is easy to derive

$$\frac{\partial \boldsymbol{\Sigma}}{\partial \mathbf{e}} = \frac{R}{X_0}\left(\frac{\partial \mathbf{X}^{\mathrm{s}}}{\partial \mathbf{e}} - \frac{1-\beta}{X_0}\mathbf{X}^{\mathrm{s}}\frac{\partial X_0}{\partial \mathbf{e}}\right) \tag{64}$$

For the elastic phase we immediately have

$$\frac{\partial \mathbf{X}^{\mathrm{s}}}{\partial \mathbf{e}} = 2GX_0\mathbb{I} \tag{65}$$

$$\frac{\partial X_0}{\partial \mathbf{e}} = \mathbf{0} \tag{66}$$

while in the plastic phase the result is far more complicated and can be found in the Appendix. For the total stress, Equation (5) provides

$$\frac{\partial \mathbf{s}}{\partial \mathbf{e}} = \frac{\partial \boldsymbol{\Sigma}}{\partial \mathbf{e}} + \frac{\partial \boldsymbol{\alpha}}{\partial \mathbf{e}} \tag{67}$$

and, recalling also Equation (60), it becomes

$$\frac{\partial \mathbf{s}}{\partial \mathbf{e}} = \frac{2G}{2G + H_{\mathrm{kin}}}\frac{\partial \boldsymbol{\Sigma}}{\partial \mathbf{e}} + \frac{2GH_{\mathrm{kin}}}{2G + H_{\mathrm{kin}}}\mathbb{I} \tag{68}$$

We also have

$$\frac{\partial \mathbf{s}}{\partial \boldsymbol{\varepsilon}} = \frac{\partial \mathbf{s}}{\partial \mathbf{e}}\frac{\partial \mathbf{e}}{\partial \boldsymbol{\varepsilon}} = \frac{\partial \mathbf{s}}{\partial \mathbf{e}}\mathbb{I}_{\mathrm{dev}} \tag{69}$$

where $\mathbb{I}_{\text{dev}}$ was already defined in (21). Taking into account the volumetric part of the stress, from Equations (1)–(3), we obtain the tangent matrix

$$\frac{\partial \boldsymbol{\sigma}}{\partial \boldsymbol{\varepsilon}} = \frac{\partial \mathbf{s}}{\partial \boldsymbol{\varepsilon}} + K(\mathbf{i}\,\mathbf{i}^{\mathrm{T}}) \tag{70}$$

Joining statements (68)–(70) we obtain

$$\mathbb{D}_{\text{disc}} = \frac{\partial \boldsymbol{\sigma}}{\partial \boldsymbol{\varepsilon}} = \frac{2G}{2G + H_{\text{kin}}} \frac{\partial \boldsymbol{\Sigma}}{\partial \mathbf{e}} \mathbb{I}_{\text{dev}} + \frac{2G H_{\text{kin}}}{2G + H_{\text{kin}}} \mathbb{I}_{\text{dev}} + K(\mathbf{i}\,\mathbf{i}^{\mathrm{T}}) \tag{71}$$

which in the elastic case simplifies to the usual

$$\mathbb{D}^{\text{e}}_{\text{disc}} = \frac{\partial \boldsymbol{\sigma}}{\partial \boldsymbol{\varepsilon}} = 2G\mathbb{I}_{\text{dev}} + K(\mathbf{i}\,\mathbf{i}^{\mathrm{T}}) \tag{72}$$

and in the plastic one can be calculated using (64) and substituting the matrix $\partial \mathbf{X}^{\text{s}}/\partial \mathbf{e}$ and the vector $\partial X_0/\partial \mathbf{e}$, which are found in Appendix.

6. A DIFFERENT MODEL FORMULATION

For completeness, we here introduce a brief review of the 'non-consistent' numerical method proposed in Reference [2].

Choosing, instead of (31), an integrating factor $X_0(\gamma)$ in the form

$$X_0(\gamma) = \begin{cases} \left(1 + \dfrac{H_{\text{iso}}}{\sigma_{\text{y},0}}\,\gamma\right)^{\frac{2G+H_{\text{kin}}}{H_{\text{iso}}}} & \text{if } H_{\text{iso}} \neq 0 \\ \exp\left(\dfrac{2G + H_{\text{kin}}}{\sigma_{\text{y},0}}\,\gamma\right) & \text{if } H_{\text{iso}} = 0 \end{cases} \tag{73}$$

it can be checked easily that a relationship similar to (33) still holds

$$\frac{\mathrm{d}}{\mathrm{d}t}[X_0 \boldsymbol{\Sigma}] = 2G\dot{\mathbf{e}} X_0 \tag{74}$$

Henceforth, defining the generalized stress vector directly as

$$\mathbf{X} = \begin{pmatrix} X_0 \boldsymbol{\Sigma} \\ X_0 \end{pmatrix} = \begin{pmatrix} \mathbf{X}^{\text{s}} \\ X_0 \end{pmatrix} \tag{75}$$

from (74) one obtains

$$\dot{\mathbf{X}}^{\text{s}} = 2G X_0 \dot{\mathbf{e}} \tag{76}$$

After some calculations similar to those of Section 4, the evolution law for $X_0(\gamma)$ reads

$$\dot{X}_0 = 0 \quad \text{(elastic phase)} \tag{77}$$

$$\dot{X}_0 = 2G\chi\dot{\mathbf{e}}^{\mathrm{T}}\mathbf{X}^{\mathrm{s}} \quad \text{(plastic phase)} \tag{78}$$

with the position

$$\chi = \chi(X_0) = \frac{2G + H_{\mathrm{kin}}}{\sigma_{\mathrm{y},0}^2(2G + H_{\mathrm{kin}} + H_{\mathrm{iso}})}\,(X_0)^{\frac{-2H_{\mathrm{iso}}}{2G+H_{\mathrm{kin}}}} \tag{79}$$

The evolution law for the generalized stress vector follows from Equations (76)–(78) and has still the form

$$\dot{\mathbf{X}} = \mathbb{A}\mathbf{X} \tag{80}$$

where now the matrix is

$$\mathbb{A} = 2G\begin{pmatrix} \mathbf{0}_{6\times 6} & \dot{\mathbf{e}} \\ \mathbf{0}_{1\times 6} & 0 \end{pmatrix} \quad \text{(elastic phase)} \tag{81}$$

$$\mathbb{A} = 2G\begin{pmatrix} \mathbf{0}_{6\times 6} & \dot{\mathbf{e}} \\ \chi\dot{\mathbf{e}}^{\mathrm{T}} & 0 \end{pmatrix} \quad \text{(plastic phase)} \tag{82}$$

At every time step the numerical scheme is as follows:

(1) Suppose the step to be elastic and compute trial values following an elastic law:

$$\mathbf{X}_{n+1}^{\mathrm{TR}} = \bar{\mathbb{G}}_{\mathrm{e}}\mathbf{X}_n \tag{83}$$

where the matrix $\bar{\mathbb{G}}_{\mathrm{e}}$, now, is given by

$$\bar{\mathbb{G}}_{\mathrm{e}} = \begin{pmatrix} \mathbb{I} & 2G\Delta\mathbf{e} \\ 0 & 1 \end{pmatrix} \tag{84}$$

If the trail solution is admissible, i.e.

$$\|\mathbf{X}_{n+1}^{\mathrm{TR}}\| \leqslant \sigma_{\mathrm{y},0}(X_{0,n+1}^{\mathrm{TR}})^{\frac{H_{\mathrm{iso}}+H_{\mathrm{kin}}+2G}{2G+H_{\mathrm{kin}}}} \tag{85}$$

then the variable values at the time step t_{n+1} are taken as the trial one just calculated.

(2) If the trial solution is non-admissible, i.e. Equation (53) is violated, then the parameter α is given by the usual formula

$$\alpha = \frac{\sqrt{C^2 - DM} - C}{D} \tag{86}$$

while the coefficients C, D, M admit the following expression

$$\begin{cases} C = 2GX_{0,n}(\mathbf{X}_n^{\mathrm{s}})^{\mathrm{T}}\Delta\mathbf{e} \\ D = (2GX_{0,n}\ \|\Delta\mathbf{e}\|)^2 \\ M = \|\mathbf{X}_n^{\mathrm{s}}\|^2 - \sigma_{\mathrm{y},0}^2(X_{0,n})^{2\varphi} \\ \varphi = \dfrac{2G + H_{\mathrm{kin}} + H_{\mathrm{iso}}}{2G + H_{\mathrm{kin}}} \end{cases} \tag{87}$$

The updating of $\mathbf{X}_{n+1}$ is still performed in two steps.

– Calculate $\mathbf{X}_{n+1}^{\mathrm{TR}}$ following an elastic law:

$$\mathbf{X}_{n+1}^{\mathrm{TR}} = \bar{\mathbb{G}}_{\mathrm{e}}\mathbf{X}_n \tag{88}$$

with $\bar{\mathbb{G}}_{\mathrm{e}}$ given by (84), *but* where $\Delta\mathbf{e} = \alpha(\mathbf{e}_{n+1} - \mathbf{e}_n)$ instead of $\Delta\mathbf{e} = (\mathbf{e}_{n+1} - \mathbf{e}_n)$

– Calculate $\mathbf{X}_{n+1}$ evolving from the new initial data $\mathbf{X}_{n+1}^{\mathrm{TR}}$ following a plastic law:

$$\mathbf{X}_{n+1} = \bar{\mathbb{G}}_{\mathrm{p}}\mathbf{X}_{n+1}^{\mathrm{TR}} \tag{89}$$

with $\bar{\mathbb{G}}_{\mathrm{p}}$ given by

$$\bar{\mathbb{G}}_{\mathrm{p}} = \begin{pmatrix} \mathbb{I} + \left[\dfrac{(a-1)}{\|\Delta\mathbf{e}\|^2}\right]\Delta\mathbf{e}\Delta\mathbf{e}^{\mathrm{T}} & \dfrac{b}{\sqrt{\chi}}\dfrac{\Delta\mathbf{e}}{\|\Delta\mathbf{e}\|} \\ b\sqrt{\chi}\dfrac{\Delta\mathbf{e}^{\mathrm{T}}}{\|\Delta\mathbf{e}\|} & a \end{pmatrix} \tag{90}$$

with $\Delta\mathbf{e} = (1-\alpha)(\mathbf{e}_{n+1} - \mathbf{e}_n)$ instead of $\Delta\mathbf{e} = (\mathbf{e}_{n+1} - \mathbf{e}_n)$.
In matrix (90), now, the scalars a and b are given by

$$a = \cosh(2G\sqrt{\chi}\ \|\Delta\mathbf{e}\|) \tag{91}$$

$$b = \sinh(2G\sqrt{\chi}\ \|\Delta\mathbf{e}\|) \tag{92}$$

(3) Finally, at the end of each step update the constant $\chi = \chi(X_{0,n+1})$ used for the calculation of the matrix $\bar{\mathbb{G}}_{\mathrm{p}}$.

Whenever needed, the relative stress and backstress can be calculated as

$$\boldsymbol{\Sigma} = \frac{\mathbf{X}^{\mathrm{s}}}{X_0} \tag{93}$$

$$\boldsymbol{\alpha} = H_{\mathrm{kin}}\mathbf{e}^{\mathrm{p}} = H_{\mathrm{kin}}\frac{2G\mathbf{e} - \boldsymbol{\Sigma}}{2G + H_{\mathrm{kin}}} \tag{94}$$

The first one is immediately obtained from the definition of $\mathbf{X}$, while the second one follows from (4) and (5), observing that $\boldsymbol{\alpha} = H_{\text{kin}}\mathbf{e}^{\text{p}}$.

The algorithmically consistent tangent matrix can be found in Reference [2]. Note that also this algorithm is exact whenever no isotropic hardening is assumed. Finally, we observe that both the considerations of Remark 4 still apply to this algorithm.

6.1. Enforced consistency variant

As it will be clear from the numerical tests of Section 7, when compared to the return map and to the algorithm of Section 4, this method shows far better accuracy properties. On the other hand, as already observed in Reference [2], the algorithm presented above is not consistent with the yield surface condition. In other words, at the end of plastic steps condition (44) does not hold exactly for the numerical solution.

Apart from physical considerations, the above property is important also for the stability of the algorithm; whenever the numerical relative stress $\boldsymbol{\Sigma}$ falls out of the numerical yield domain (i.e. $\|\boldsymbol{\Sigma}_{n+1}\| > R_{n+1}$) this may lead to instabilities in the following time step. Therefore, in practical finite element applications, it is recommendable to enforce the consistency using a radial projection on the surface in each time step in which $\|\boldsymbol{\Sigma}\| > R$ (simply multiply the relative stresses $\boldsymbol{\Sigma}$ by the rate $R/\|\boldsymbol{\Sigma}\|$). This consistency check can be done at the start of each step (which allows to use the same algorithmic tangent matrix) or at the end of each step. For simplicity, in the numerical tests presented in Section 7 we consider the first case.

As the numerical tests will show, this 'enforced consistency' algorithm still retains the good accuracy properties of its original counterpart.

7. NUMERICAL TESTS AND COMPARISON ISSUES ON THE METHODS

We now investigate the validity of the three exponentially based algorithms of the previous sections, also in comparison with the classical radial return map method. Accordingly, the four considered methods are:

- **RRM** Radial Return Map method (Section 3)
- **ESC** Exponential Symmetric Consistent method (Section 4)
- **ENN** Exponential Non-symmetric Non-consistent method ([2] and Section 6)
- **ENC** Exponential Non-symmetric Consistent method (Section 6.1)

The numerical investigations are divided in two parts. In order to test the algorithm accuracy, in Section 7.1 we consider three pointwise stress–strain load histories with different time discretizations, and plot the respective error graphs. Instead, to test the algorithm performance and Newton iteration convergence, in Section 7.2 we consider two classical initial boundary value problems.

Finally, in Section 7.3 we present a systematic comparison of the four methods in terms of yield consistency and accuracy, analysing the capability to provide exact solutions for pure proportional loading and in the case of elasto-plastic materials with linear kinematic hardening only.

In this analysis we adopt two distinct sets of material constants

- Material 1 (see Reference [7])

$$E = 100\,\text{MPa} \quad v = 0.3 H_{\text{kin}} = 10\,\text{MPa} \quad H_{\text{iso}} = 10\,\text{MPa} \quad \sigma_{\text{y},0} = 15\,\text{MPa}$$

- Material 2 (see Reference [8])

$$E = 7000\,\text{MPa} \quad v = 0.3 H_{\text{kin}} = 0\,\text{MPa} \quad H_{\text{iso}} = 225\,\text{MPa} \quad \sigma_{\text{y},0} = 24.3\,\text{MPa}$$

where we recall that the Young Modulus E and the Poisson ratio v uniquely determine the constants

$$K = \frac{E}{3(1-2v)} \quad G = \frac{E}{2(1+v)} \tag{95}$$

The pointwise numerical tests are performed with the aid of the CE-Driver (see Reference [11]), while the boundary value problems are solved using the finite element code FEAP (see Reference [12]).

7.1. Pointwise stress–strain tests

We consider three biaxial non-proportional stress–strain histories, graphically represented in Figure 1. The loading histories are obtained assuming to control the two strain components indicated in the figure and requiring that all the stress components not corresponding to the two controlled strain components are identically equal to zero. In particular, in the three biaxial problems we control the following strain components:

$$\begin{aligned} &\text{Problem 1:} \quad \boldsymbol{\varepsilon}_{11} \quad \boldsymbol{\varepsilon}_{12} \\ &\text{Problem 2:} \quad \boldsymbol{\varepsilon}_{11} \quad \boldsymbol{\varepsilon}_{22} \\ &\text{Problem 3:} \quad \boldsymbol{\varepsilon}_{11} \quad \boldsymbol{\varepsilon}_{12} \end{aligned}$$

which are varied proportionally to the strain value

$$\boldsymbol{\varepsilon}_{\text{y, mono}} = \frac{\sqrt{3}\sigma_{\text{y},0}}{2E} \tag{96}$$

corresponding to the first yielding in a mono-axial stress–strain history.

Lacking the analytical solution of the problems under investigation, we compute the 'exact' solutions using the return map method with a very fine time interval, corresponding to 50 000 steps per second [$\Delta t = 0.00002$ s]. Such 'exact' solutions are compared with the 'numerical' ones, corresponding, respectively, to 10, 20 and 40 steps per second [$\Delta t = 0.1, 0.05, 0.025$ s], i.e. obtained with more practical time discretizations.

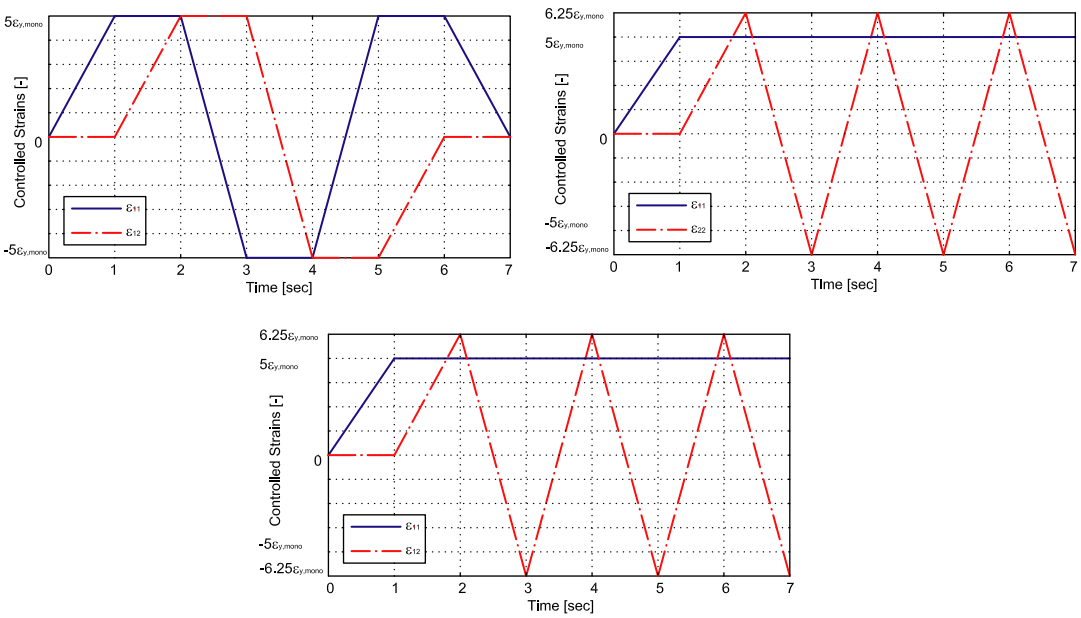

Figure 1. Pointwise stress–strain load histories.

The error is evaluated separately for the stress and the strain; for the stresses, we introduced the following relative norm:

$$E_n = \frac{\| \mathbf{v}_n - \bar{\mathbf{v}}_n \|}{R_n} \tag{97}$$

where $\| \bullet \|$ indicates the usual ℓ^2 vector norm, R_n is the yield surface radius at time t_n, and $\mathbf{v}_n$ and $\bar{\mathbf{v}}_n$ are vectors, containing, respectively, the 'exact' and the 'numerical' solution at time t_n. For the strains we use the same relative norm scaled by $2G$.

The error measure (97) is used due to the high variation of the problem solution, which makes inappropriate the use of the classical relative error

$$\hat{E}_n = \frac{\| \mathbf{v}_n - \bar{\mathbf{v}}_n \|}{\| \mathbf{v}_n \|} \tag{98}$$

Figures 2–4 report stress and strain relative errors (97) using Material 1 for the first load history, for the three different time discretizations indicated above. Figures 5–7 report the same quantities but for the third load history, while Figures 8–13 repeat the process with material constants Material 2. For the sake of brevity we decided not to report the error graphs corresponding to the second load history since they show qualitatively similar results. From the error plots, we can extract the following comments:

- The ESC and the RRM methods perform similarly in terms of error, although in general the ESC seems slightly better. As the step size is reduced, both methods seem to converge with linear accuracy, i.e. the error seems to be divided by 2 every time we double the number of steps (error goes as Δt).

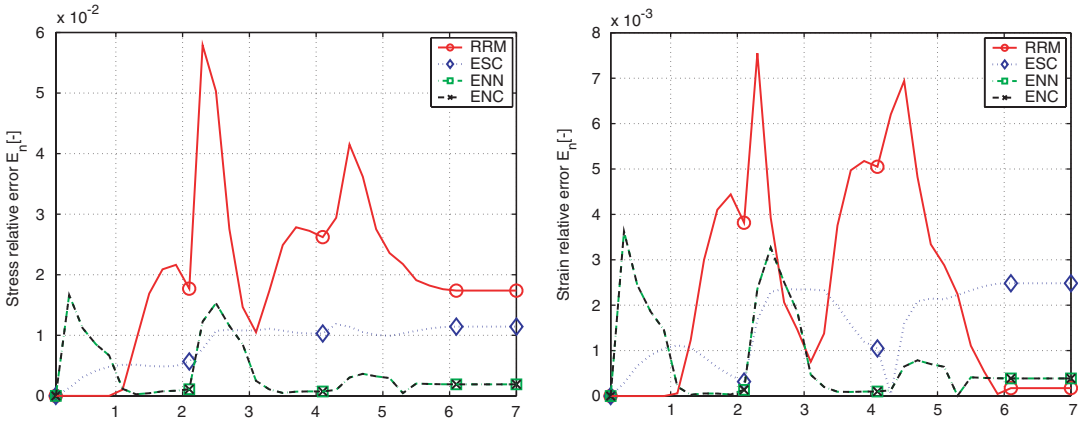

Figure 2. Problem 1—Material 1—stress and strain error—$\Delta t = 0.1$.

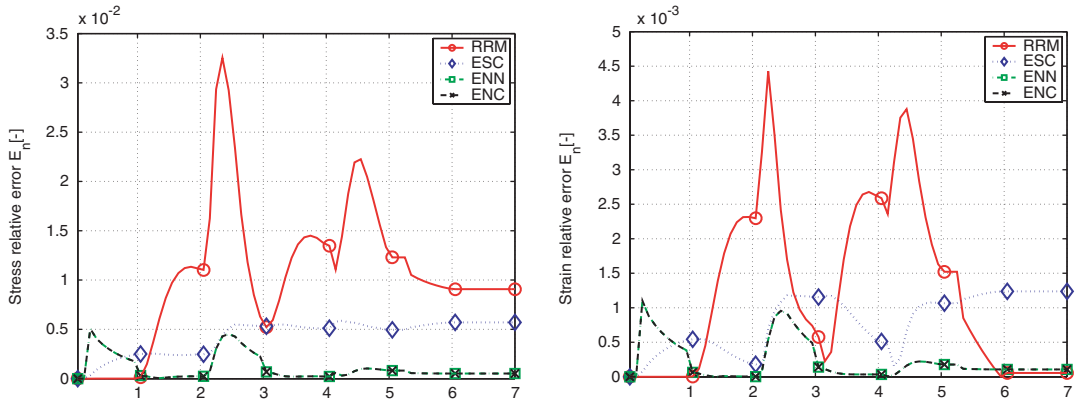

Figure 3. Problem 1—Material 1—stress and strain error—$\Delta t = 0.05$.

- The error of the non-symmetric methods ENN and ENC is decisively better than one of the other two algorithms; in this case the error is roughly divided by 4 every time we double the number of steps (error goes as $(\Delta t)^2$).

In order to better investigate the rate of convergence of the method, we introduce the *total error* as the ℓ^1 norm in time of the absolute error:

$$E_{\mathrm{T}} = \sum_{n=1}^{N} \Delta t \, \| \mathbf{v}_n - \bar{\mathbf{v}}_n \| \tag{99}$$

where $\mathbf{v}_n$ and $\bar{\mathbf{v}}_n$ are defined as in relation (97). Then, in Figure 14 we plot the total error versus the number of grid steps in logarithmic scale for the four methods RRM, ESC, ENC and ENN, for the first load history and with Material 1. The quadratic convergence of the ENC and the ENN, with respect to the linear one of the other algorithms, can be clearly appreciated.

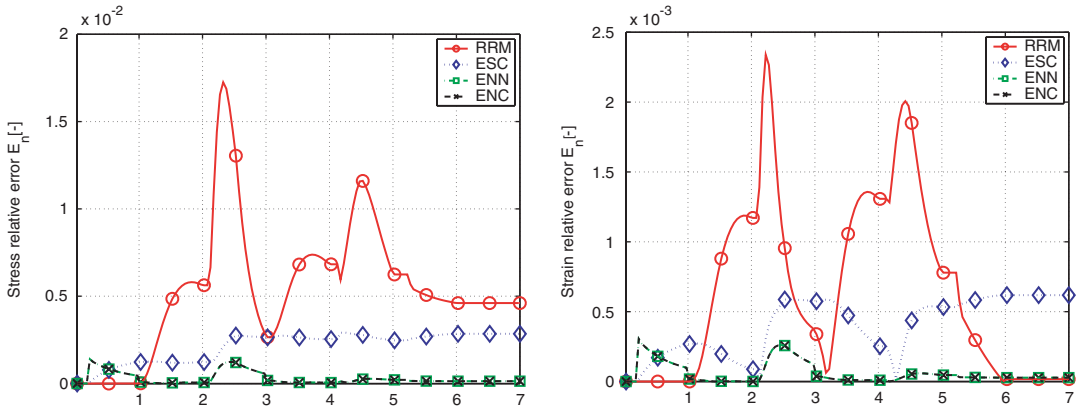

Figure 4. Problem 1—Material 1—stress and strain error—$\Delta t = 0.025$.

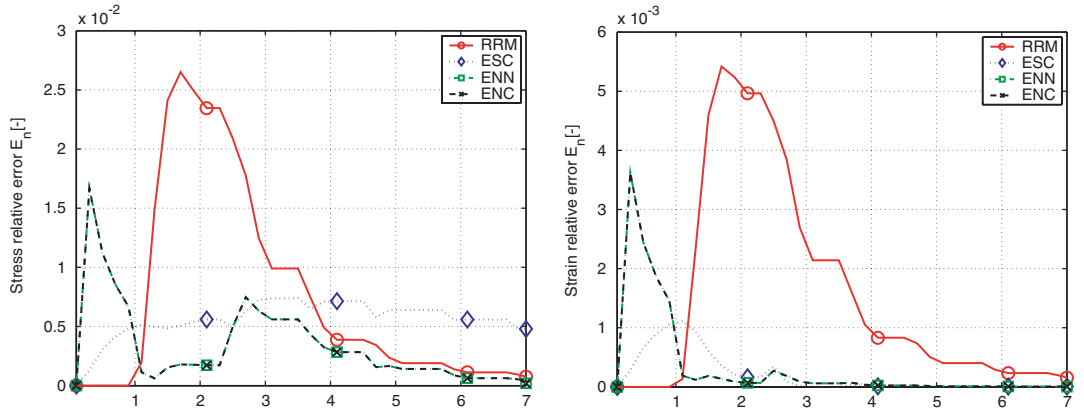

Figure 5. Problem 3—Material 1—stress and strain error—$\Delta t = 0.1$.

A further *detailed comparison* of the four methods in terms of intrinsic numerical properties is presented in Section 7.3.

7.2. Two initial boundary value problems

We consider two 3-dimensional thin rectangular perforated strips, subject to uniaxial extension in a plane strain state [5]. The first strip has a circular hole in the centre, while the second one an elliptical hole. Both strips have three planes of symmetry and in Figure 15 we show one quarter of the domain for each of the two strips. The geometric lengths referred to Figure 15 are

$$B = 100\,\text{mm}, \quad H = 180\,\text{mm}, \quad R = 50\,\text{mm}, \quad H_0 = 10\,\text{mm}, \quad B_0 = 50\,\text{mm}$$

while the thickness is 10 mm.

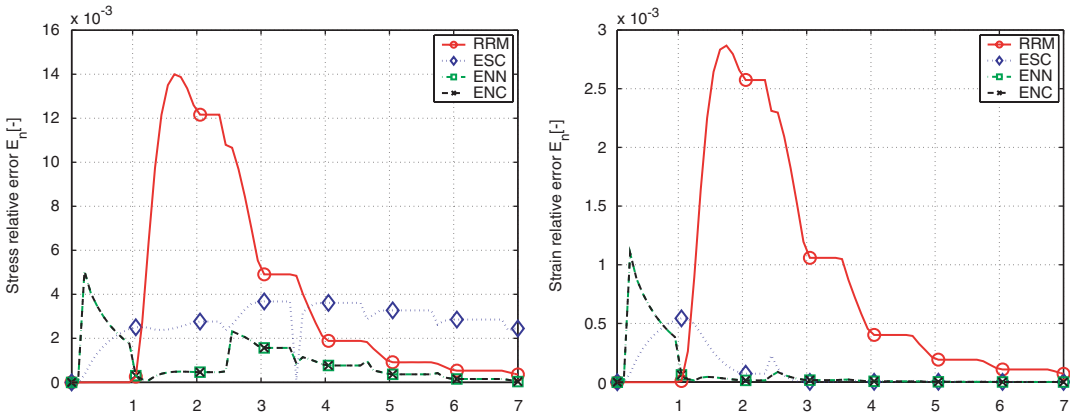

Figure 6. Problem 3—Material 1—stress and strain error—$\Delta t = 0.05$.

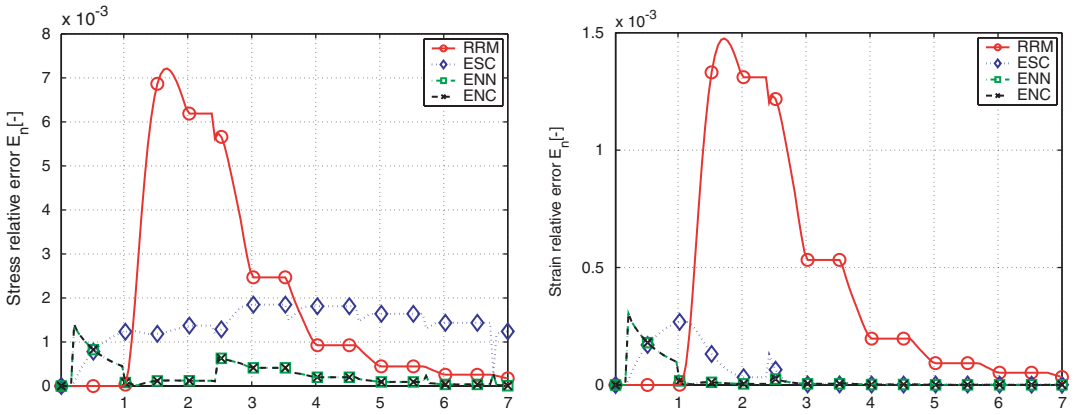

Figure 7. Problem 3—Material 1—stress and strain error—$\Delta t = 0.025$.

In the analysis we consider both Materials 1 and 2 as previously done, so that a total of four cases (two material sets for each strip) are investigated. The problem loading histories are composed of a first phase (1 s), in which, controlling the displacements, the strip is stretched assigning a top vertical displacement of $\delta_{\max}$ and a second phase (1 s) in which the imposed displacement is set back to 0 mm. In the case of Material 1 we set $\delta_{\max} = 40$ mm, while for Material 2 we set $\delta_{\max} = 5$ mm.

We solve the boundary value problems using the multi-purpose finite element code FEAP [12], in which we implemented each of the four aforementioned methods.

Due to geometry and loading symmetry, we solve the problem only on a quarter of the original domain (Figure 16), using 192 displacement-based brick elements. As simulations output, we counted the number of residual evaluations per time step (i.e. number of Newton iterations per time step). The results are reported in Tables I–II (first strip) and III–IV (second strip) in terms of the average number of iterations per single step. As it can be seen the

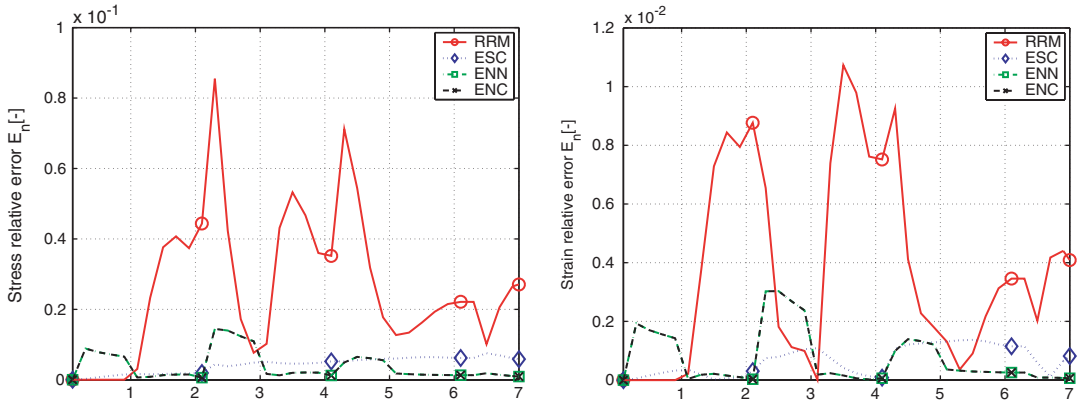

Figure 8. Problem 1—Material 2—stress and strain error—$\Delta t = 0.1$.

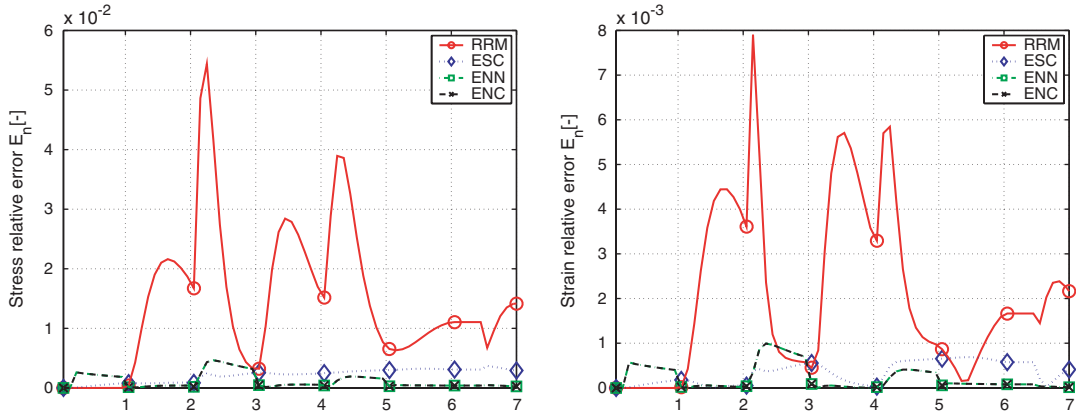

Figure 9. Problem 1—Material 2—stress and strain error—$\Delta t = 0.05$.

Newton convergence speeds of the exponential based methods are similar and comparable to the one relative to the return map, even if this latter method behaves slightly better.

Finally, for both strips we monitor the displacements of point A (Figure 15), assuming that this is a good indicator on how the problem is actually approximated by the numerical methods. This comparison is performed between the two linear converging methods, i.e. the RRM and the ESC. In Table V, we report the total modified relative error for the horizontal displacement at point A, between a discrete solution with variable number of steps and an 'exact' solution obtained with the RRM with 50 000 steps per second, i.e.

$$\tilde{E}_n = \sum_{n=1}^{N} \frac{|\, D_n - \bar{D}_n \,|\, \Delta t}{\sup_{j\in\{0,1,\ldots,n\}} |\, D_j \,|} \tag{100}$$

where D_n is the described displacement at time t_n calculated with the discrete method, while $\bar{D}_n$ is the one obtained with the 'exact' solution.

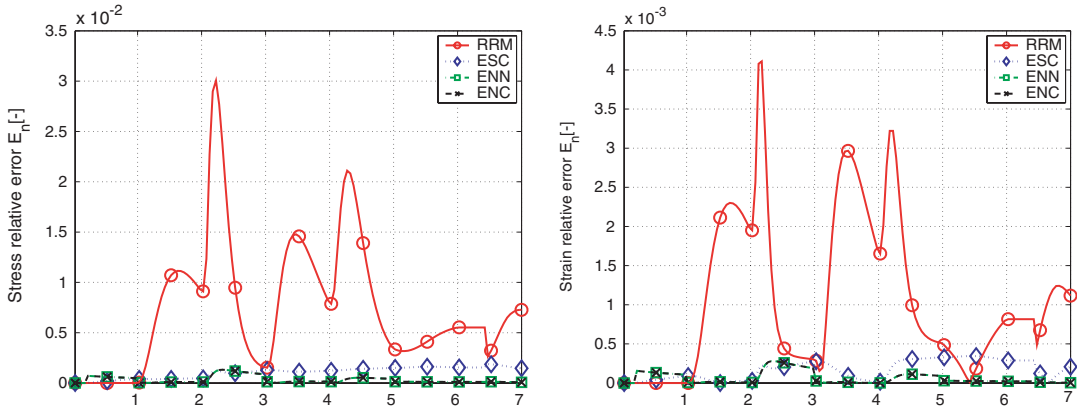

Figure 10. Problem 1—Material 2—stress and strain error—$\Delta t = 0.025$.

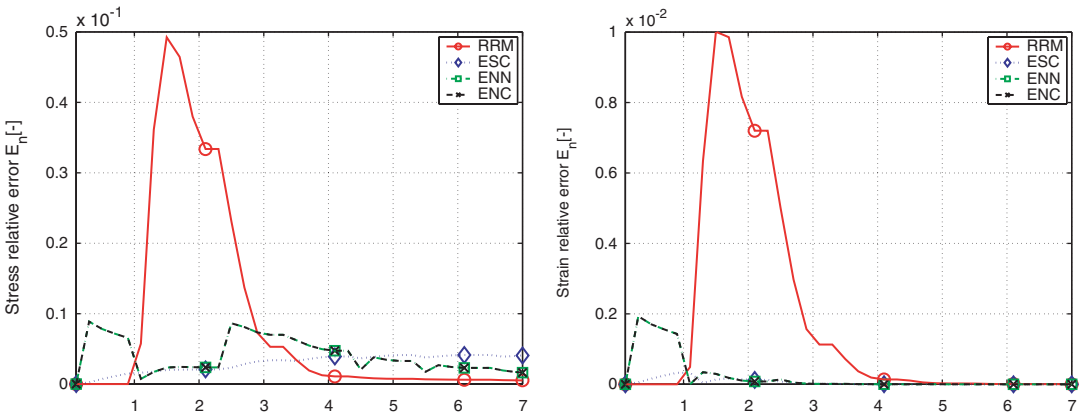

Figure 11. Problem 3—Material 2—stress and strain error—$\Delta t = 0.1$.

From Table V it can be seen that the behaviour of the two methods is roughly equivalent, although not identical; as it could be reasonably expected, both methods show linear convergence also in the global problem.

7.3. Additional comparisons between the four methods

In this section we make some additional observations and comparisons on the four methods considered in the paper. In particular, we are interested in the following four properties:

- *Consistency of the yield condition*
- *Order of accuracy*
- *Exactness for* $R = \text{const}$ (*no isotropic hardening*)
- *Exactness for* $\mathbf{n} = \text{const}$ (*proportional loading*)

The investigation results are discussed in detail in the following and are summarized in Table VI.

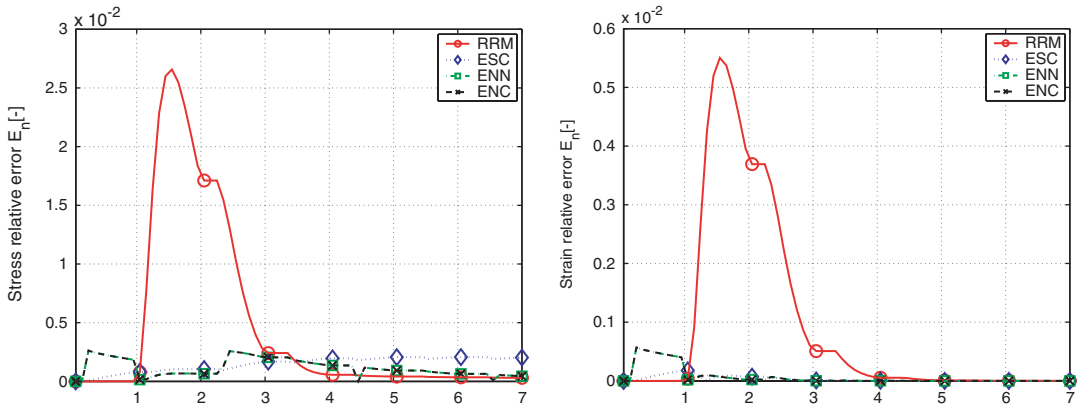

Figure 12. Problem 3—Material 2—stress and strain error—$\Delta t = 0.05$.

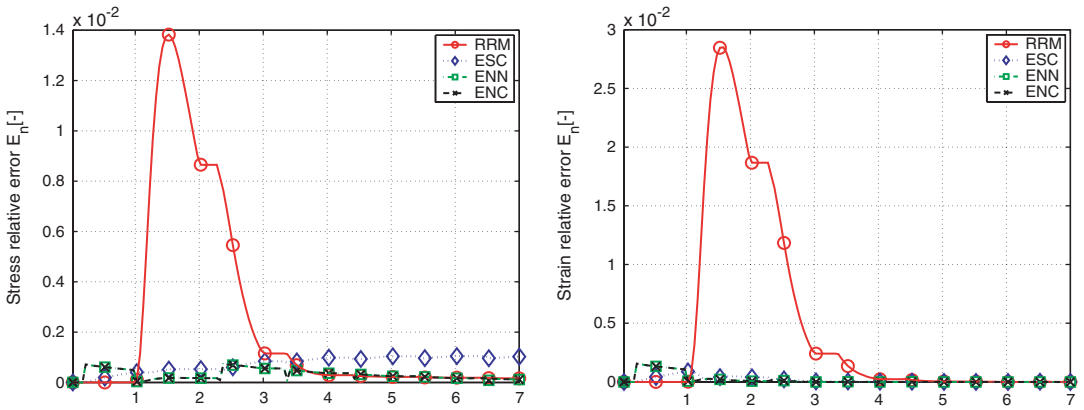

Figure 13. Problem 3—Material 2—stress and strain error—$\Delta t = 0.025$.

Consistency of the yield condition: As already underlined, the consistency with the yield condition during plastic steps is a key property for the stability of the algorithm in practical applications. The RRM, ESC and ENC algorithms satisfy this condition. While for the ESC algorithm the yield consistency is naturally satisfied due to its specific formulation, the same does not hold true for the other two methods; in the RRM and ESC algorithms the consistency condition is enforced projecting the stress solution on the yield surface at every time step.

Order of accuracy: As shown in the numerical tests, all the listed algorithms hold at least linear accuracy. This can also be easily proved calculating an asymptotic expansion of the truncation error in the standard way. The methods which instead show quadratic accuracy are the ENN and its variant ENC. This quadratic accuracy is evident from all the numerical tests performed but cannot be proved directly by standard means, because it is caused by a coupling of two phenomena from one time step to the other. In *rough words*, what

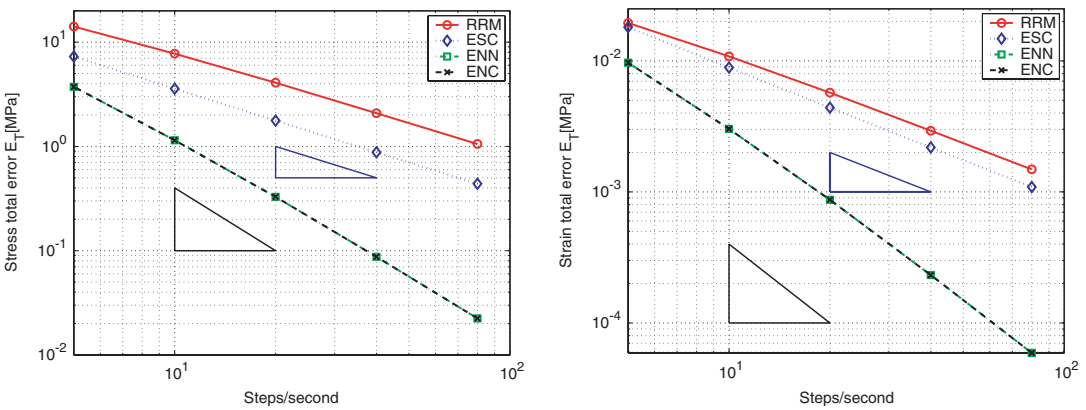

Figure 14. Problem 1—Material 1—stress and strain total error versus time step size.

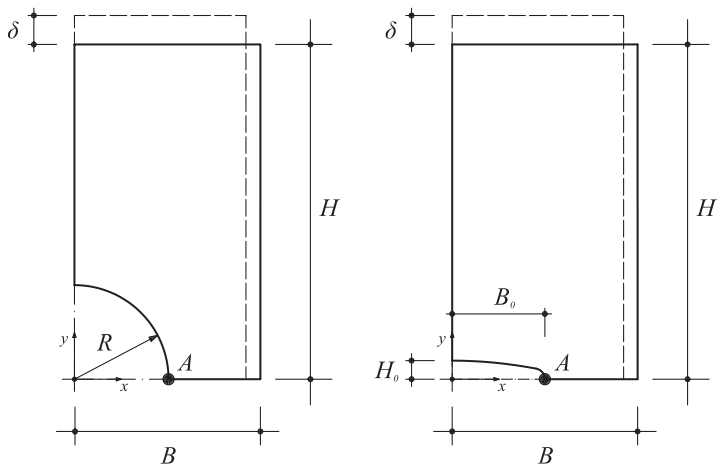

Figure 15. Strips with circular and elliptical holes: geometry and imposed displacements for a single quarter of the strips.

happens is:

- in each single time step, the radius of the discrete yield surface grows more than the norm of the discrete relative stress $\mathbf{\Sigma}$; therefore, at the end of each plastic steps, $\mathbf{\Sigma}$ lays inside (and not on the surface of) the yield sphere. As a consequence, in the following step the relative stress $\mathbf{\Sigma}$ must reach the yield surface before any isotropic hardening (i.e. 'growth radius') phenomena can be activated
- for sufficiently small Δt, whenever an isotropic hardening effect is activated, the discrete radius grows more than the radius of the continuous problem

The coupling of these two opposite effects seems to enhance the accuracy of the method.

Table I. First b.v.p.—Material 1—average number of iterations per time step.

Method	Δt (s) 0.1	0.01	0.001
RRM	3.25	2.83	2.73
ESC	4.30	3.17	2.90
ENN	4.30	3.17	2.91
ENC	4.30	3.17	2.90

Table II. First b.v.p.—Material 2—average number of iterations per time step.

Method	Δt (s) 0.01	0.001	0.0001
RRM	4.90	4.28	3.68
ESC	7.21	4.97	4.30
ENN	7.18	4.96	4.28
ENC	7.21	4.97	4.30

Table III. Second b.v.p.—Material 1—average number of iterations per time step.

Method	Δt (s) 0.1	0.01	0.001
RRM	3.65	3.18	2.95
ESC	4.70	3.66	3.27
ENN	4.85	3.70	3.33
ENC	4.70	3.66	3.27

Table IV. Second b.v.p.—Material 1—average number of iterations per time step.

Method	Δt (s) 0.01	0.001	0.0001
RRM	5.00	4.33	3.75
ESC	7.72	5.16	4.42
ENN	7.71	5.17	4.45
ENC	7.72	5.16	4.42

Exactness in case of no isotropic hardening: All the exponential-based methods here analysed (ESC, ENN, ENC) share the important property of solving exactly the problem whenever there is no isotropic hardening in the model, as observed in Sections 4 and 6. Clearly, this property

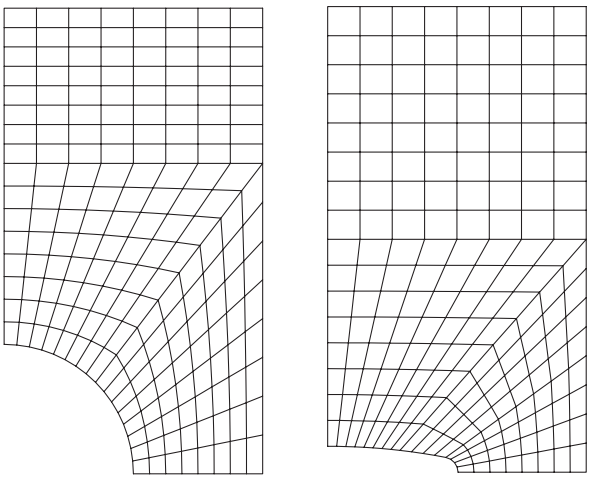

Figure 16. Strips with circular and elliptical holes: plane projection of the adopted meshes.

Table V. Point displacement total error versus time step size for the first two problems using the ESC and the RRM.

b.v.p.	Steps/second	Total error RRM $[\times 10^{-2}]$	Total error ESC $[\times 10^{-2}]$
Problem 1—Material 1	10	6.13×10^{-2}	1.20×10^{-1}
	100	1.04×10^{-2}	0.94×10^{-2}
	1000	1.01×10^{-3}	0.83×10^{-3}
Problem 1—Material 2	100	4.26×10^{-2}	7.33×10^{-2}
	1000	4.24×10^{-3}	6.46×10^{-3}
	10000	3.44×10^{-4}	6.74×10^{-4}
Problem 2—Material 1	10	4.34×10^{-1}	8.07×10^{-2}
	100	4.45×10^{-2}	5.18×10^{-3}
	1000	4.19×10^{-3}	5.64×10^{-4}
Problem 2—Material 2	100	1.54×10^{-1}	1.19×10^{-1}
	1000	1.56×10^{-2}	1.31×10^{-2}
	10000	1.56×10^{-3}	1.33×10^{-3}

is not owned by the radial return map method. For knowledge on other exact methods in the engineering literature, see for instance References [13, 14] and also References [15–17].

Exactness in case of proportional loading: The radial return map method holds the following interesting property. Whenever in a given plastic time step $\dot{\mathbf{e}}$ is constant and parallel to the

Table VI. Comparison of the four methods on some important algorithmic properties.

	RRM	ESC	ENN	ENC
Consistency of the yield condition	$\surd$	$\surd$	$\times$	$\surd$
Order of accuracy	1	1	2	2
Exactness for $R = \text{const}$ (no isotropic hardening)	$\times$	$\surd$	$\surd$	$\surd$
Exactness for $\mathbf{n} = \text{const}$ (proportional loading)	$\surd$	$\times$	$\times$	$\times$

normal direction $\mathbf{n}$, the numerical solution furnished by the algorithm coincides with the exact one. This follows easily observing that in such particular case the yield radius R possesses a linear evolution law in time

$$\begin{aligned} \dot{R} &= \frac{2G\,H_{\text{iso}}}{2G + H_{\text{kin}} + H_{\text{iso}}}\,\|\dot{\mathbf{e}}\| \\ R_{n+1} &= R_n + \frac{2G\,H_{\text{iso}}}{2G + H_{\text{kin}} + H_{\text{iso}}}\,\|\dot{\mathbf{e}}\|\,\Delta t \end{aligned} \tag{101}$$

which is clearly solved exactly by backward Euler methods. This property is instead not shared by the exponential map methods analysed here.

Remark 5

Liu in Reference [10] proposed to adopt the Cayley transform method (see for example Reference [18] and reference therein) to solve Equation (40). In our case, this amounts to the following update scheme for a plastic step:

$$\mathbf{X}_{n+1} = \begin{pmatrix} \mathbb{I} + \left[\dfrac{2G^2}{\Theta}\right]\Delta\mathbf{e}\Delta\mathbf{e}^{\mathrm{T}} & \left[\dfrac{2GR_n}{\Theta}\right]\Delta\mathbf{e} \\ \left[\dfrac{2GR_n}{\Theta}\right]\Delta\mathbf{e}^{\mathrm{T}} & \dfrac{R_n^2 + G^2\,\|\Delta\mathbf{e}\|^2}{R^*} \end{pmatrix}\mathbf{X}_n \tag{102}$$

with

$$\Theta = R_n^2 - G^2\,\|\Delta\mathbf{e}\|^2 \tag{103}$$

Indeed, it can be proved that the Cayley method applied to our system would give both a quadratic and a naturally consistent method; therefore it seems an optimal candidate to solve an equation of type (40).

On the other side, the Cayley transform method can be applied only provided that

$$\Theta > 0 \iff \|\Delta\mathbf{e}\| < \frac{R_n}{G} \tag{104}$$

which makes the method almost useless in practical cases. The reasons are twofold. First, for realistic materials the ratio $\sigma_{\text{y},0}/G$ can easily reach values around 10^{-2}, which means that

even for pointwise strain driven tests the required Δt may be rather small. But even worst, when a Newton–Raphson (or other) strategy is adopted to solve a global plastic deformation problem, the user has no direct control on Θ; therefore condition (104) cannot be guaranteed. For example, in the global problems solved in Section 7.2 the value $(G/R_n) \parallel \Delta \mathbf{e} \parallel$ (which in order to adopt a Cayley method should be lesser than one) easily reached values over 100 on some points of the mesh. This is the reason why the authors avoided adopting a Cayley method in order to solve Equation (40).

8. CONCLUSIONS

We presented a new numerical method for the solution of the associative von-Mises elasto-plastic constitutive law with linear kinematic and isotropic hardening. This method (ESC) can be considered a naturally consistent evolution of the method ENN proposed in Reference [2]. Also, we presented a variant of the non-yield-consistent method ENN in which the yield consistency condition is enforced by radial projection (ENC). In the present paper all these methods are subjected to extensive numerical tests, comparing the performances also with the well established radial return map algorithm. The comparisons were performed considering both purely constitutive pointwise tests and initial boundary value problems.

Although naturally consistent, the new ESC method looses the quadratic accuracy which is a key property of the ENN method. On the other side, the yield condition consistency is a very important property in applications. Therefore, between the three exponential based methods considered, probably the best one turns out to be the ENC, which is both quadratic and consistent. When compared with the return map on a global problem, the exponential based methods seem to be less performing and need about 15% more of iterations. On the other side, the Newton convergence speed of all the methods is acceptable. Therefore, the quadratic method ENC may be a good choice when accuracy is the first requirement for the application under consideration.

Another issue that the authors are willing to address is the theoretical study of the stability and accuracy of the exponential methods. An initial study of these properties is already in progress. This is interesting also in order to establish a deeper comparison between the new class of exponential-based methods and return mapping schemes, which are well known for their good stability properties. Moreover, the authors are convinced that the new formulation of Section 4 may hopefully lead to naturally consistent methods with quadratic accuracy. Both topics will be presented in References [19, 20].

Finally, it is worth to spend some word regarding the possibility of extending this kind of methods to different plastic constitutive laws. The authors are convinced that extensions/modifications still based on a von Mises spherical yield surface (for example, non-linear hardening laws) can be in general treated following the same principles. A different care must be given when a non-spherical yield surface is considered, because the formulation here presented seems to rely strongly on the particular properties of the spherical manifold on which the deviatoric relative stresses develop during plastic phases. In particular, it plays a key role in the equivalence between the normal unit vector and the normalized stresses during plastic phases. On the other hand, other kinds of smooth manifolds may possess equivalent properties which would allow, perhaps after some '*ad hoc*' transformation in stress space, for a similar formulation; this may include for example the case of

elliptic yield surfaces. In general, the authors are convinced about the interest in developing methods which stem from different formulations based on inherent geometrical properties of the problem; this may constitute a valid alternative to return mapping schemes in the future.

APPENDIX

In the following we prove the consistency of the ESC method (Section 4) and present the tangent matrix of the generalized stress vector addressed in (64).

A.1. Consistency of the ESC algorithm

We want to prove that, at the end of each plastic step, for the numerical solution it holds

$$\| \boldsymbol{\Sigma}_{n+1} \| = R_{n+1} \tag{A1}$$

which, recalling (28) and (34), is equivalent to

$$\| \mathbf{X}^{\mathrm{s}}_{n+1} \|^2 - X^2_{0,\,n+1} = 0 \tag{A2}$$

In every elasto-plastic step X^{TR}_{n+1} is the extreme point of the elastic part of the step, due to its algorithmic definition (88); therefore, it is easy to check that

$$\| \mathbf{X}^{\mathrm{s,\,TR}}_{n+1} \|^2 - (X^{\mathrm{TR}}_{0,\,n+1})^2 = 0 \tag{A3}$$

The discrete generalized stress $\mathbf{X}$ evolves following the dynamical law (40) and its updating at the end of each step is performed admitting to freeze $R = R_n$ at the beginning of the time interval as already mentioned with reference to matrix (42). Due to (A3), all we have to prove in order to show that (A2) holds is that

$$\frac{\mathrm{d}}{\mathrm{d}t}(\| \mathbf{X}^{\mathrm{s}} \|^2 - X_0^2) = 0 \tag{A4}$$

during the rest of the step. First a direct time derivative of the left member, then using (40) and (42) gives

$$\frac{\mathrm{d}}{\mathrm{d}t}(\| \mathbf{X}^{\mathrm{s}} \|^2 - X_0^2) = 2(\mathbf{X}^{\mathrm{s}})^{\mathrm{T}}\dot{\mathbf{X}}^{\mathrm{s}} - 2X_0\dot{X}_0 = \frac{4G}{R_n}X_0\,(\mathbf{X}^{\mathrm{s}})^{\mathrm{T}}\dot{\mathbf{e}} - \frac{4G}{R_n}X_0(\mathbf{X}^{\mathrm{s}})^{\mathrm{T}}\dot{\mathbf{e}} = 0 \tag{A5}$$

The assertion is proved.

A.2. Tangent matrix for the generalized stress

We now present the tangent matrix $\partial\mathbf{X}^{\mathrm{s}}/\partial\mathbf{e}$ and tangent vector $\partial X_0/\partial\mathbf{e}$ for plastic phases, which, from Equation (71), provide the tangent matrix $\partial\boldsymbol{\sigma}/\partial\boldsymbol{\varepsilon}$ of the new algorithm during

plastic or mixed elasto-plastic steps. As usual, unless explicitly specified all relevant quantities are evaluated at the actual time step end, i.e. at t_{n+1}.

Remembering that purely plastic steps are a particular case within the range of mixed ones (see Section 5), we start analysing the latter. From (88)–(57), we have

$$\mathbf{X}_{n+1} = \bar{\mathbb{G}}_{\mathrm{p}} \bar{\mathbb{G}}_{\mathrm{e}} \mathbf{X}_n = \mathbb{G}_{\mathrm{p}}[(1-\alpha)\Delta\mathbf{e}]\, \mathbb{G}_{\mathrm{e}}[\alpha\Delta\mathbf{e}]\, \mathbf{X}_n \tag{A6}$$

where the above matrices are given by (49) and α (which depends on $\Delta\mathbf{e}$) is the 'elastic step proportion' defined in (54). Consequently, following basic differentiation rules, we have

$$\frac{\partial \mathbf{X}_{n+1}}{\partial \mathbf{e}} = [\tilde{\mathbb{A}}_1 + \tilde{\mathbb{A}}_2 + \tilde{\mathbb{A}}_3 + \tilde{\mathbb{A}}_4]\, \mathbf{X}_n \tag{A7}$$

where the matrices

$$\begin{aligned}
\tilde{\mathbb{A}}_1 &= \frac{\partial \mathbb{G}_{\mathrm{p}}}{\partial \Delta\mathbf{e}}[(1-\alpha)\Delta\mathbf{e}]\, \mathbb{G}_{\mathrm{e}}[\alpha\Delta\mathbf{e}] \\
\tilde{\mathbb{A}}_2 &= \frac{\partial \mathbb{G}_{\mathrm{p}}}{\partial \alpha}[(1-\alpha)\Delta\mathbf{e}] \frac{\mathrm{d}\alpha}{\mathrm{d}\Delta\mathbf{e}}[\Delta\mathbf{e}]\, \mathbb{G}_{\mathrm{e}}[\alpha\Delta\mathbf{e}] \\
\tilde{\mathbb{A}}_3 &= \mathbb{G}_{\mathrm{p}}[(1-\alpha)\Delta\mathbf{e}]\, \frac{\partial \mathbb{G}_{\mathrm{e}}}{\partial \Delta\mathbf{e}}[\alpha\Delta\mathbf{e}] \\
\tilde{\mathbb{A}}_4 &= \mathbb{G}_{\mathrm{p}}[(1-\alpha)\Delta\mathbf{e}]\, \frac{\partial \mathbb{G}_{\mathrm{e}}}{\partial\, \alpha}[\alpha\Delta\mathbf{e}] \frac{\mathrm{d}\alpha}{\mathrm{d}\Delta\mathbf{e}}[\Delta\mathbf{e}]
\end{aligned} \tag{A8}$$

From Equation (A7) we can immediately derive $\partial \mathbf{X}^{\mathrm{s}}_{n+1}/\partial \mathbf{e}$ (first 6 components) and $\partial \mathbf{X}_{0,\,n+1}/\partial \mathbf{e}$ (last component); in order to obtain the classical tangent matrix, the obtained equations must be finally expressed as a linear function of the strain derivation vector instead of in the form (A7), which is expressed as a linear function of $\mathbf{X}_n$. Doing so, we finally obtain that for mixed steps

$$\frac{\partial \mathbf{X}^{\mathrm{s}}}{\partial \mathbf{e}} = \mathbb{A}_1 + \mathbb{A}_2 + \mathbb{A}_3 + \mathbb{A}_4 \tag{A9}$$

$$\frac{\partial \mathbf{X}_0}{\partial \mathbf{e}} = \mathbf{b}_1 + \mathbf{b}_2 + \mathbf{b}_3 + \mathbf{b}_4 \tag{A10}$$

where the matrices $\mathbb{A}$ and vectors $\mathbf{b}$ are described below without addressing the calculations. For purely plastic steps, being α constantly equal to zero, we instead obtain the shorter formulation

$$\frac{\partial \mathbf{X}^{\mathrm{s}}}{\partial \mathbf{e}} = \mathbb{A}_1 \tag{A11}$$

$$\frac{\partial \mathbf{X}_0}{\partial \mathbf{e}} = \mathbf{b}_1 \tag{A12}$$

We start introducing (see again (54) for M, D, C in each step) the vector $\mathbf{v} = \mathrm{d}\alpha/\mathrm{d}\Delta\mathbf{e}$

$$\begin{aligned}
\mathbf{v} &= \phi_1 \frac{\mathrm{d}C}{\mathrm{d}\Delta\mathbf{e}} + \phi_2 \frac{\mathrm{d}D}{\mathrm{d}\Delta\mathbf{e}} \\
\phi_1 &= \frac{1}{D}\left(\frac{C}{\sqrt{C^2 - DM}} - 1\right) \\
\phi_2 &= -\frac{1}{D^2}\left(\frac{DM}{2\sqrt{C^2 - DM}} + \sqrt{C^2 - DM} - C\right) \\
\frac{\mathrm{d}C}{\mathrm{d}\Delta\mathbf{e}} &= \frac{2G}{R_n} X_{0,n}\, \mathbf{X}_n^{\mathrm{s}} \\
\frac{\mathrm{d}D}{\mathrm{d}\Delta\mathbf{e}} &= 2\left(\frac{2G}{R_n} X_{0,n}\right)^2 \Delta\mathbf{e}
\end{aligned} \tag{A13}$$

Introducing the scalars

$$\begin{aligned}
a &= \cosh\left(\frac{2G}{R_n}(1-\alpha)\,\|\,\Delta\mathbf{e}\,\|\right) \\
b &= \sinh\left(\frac{2G}{R_n}(1-\alpha)\,\|\,\Delta\mathbf{e}\,\|\right) \\
s &= \frac{\Delta\mathbf{e}\cdot\mathbf{X}_n^{\mathrm{s}}}{\|\,\Delta\mathbf{e}\,\|} \\
k &= \frac{2G}{R_n}(1-\alpha) \\
\tilde{k} &= -\frac{2G}{R_n}\,\|\,\Delta\mathbf{e}\,\|
\end{aligned} \tag{A14}$$

and the matrices

$$\mathbb{M}_1 = s\left(kb - 2\,\frac{a-1}{\|\,\Delta\mathbf{e}\,\|}\right)\left[\frac{\Delta\mathbf{e}\,\Delta\mathbf{e}^{\mathrm{T}}}{\|\,\Delta\mathbf{e}\,\|^2}\right] + \frac{(a-1)s}{\|\,\Delta\mathbf{e}\,\|}\,\mathbb{I} + \frac{a-1}{\|\,\Delta\mathbf{e}\,\|}\left[\frac{\Delta\mathbf{e}\,\mathbf{X}_n^{\mathrm{s}\,\mathrm{T}}}{\|\,\Delta\mathbf{e}\,\|}\right] \tag{A15}$$

$$\mathbb{M}_2 = \left(ka - \frac{b}{\|\,\Delta\mathbf{e}\,\|}\right)\left[\frac{\Delta\mathbf{e}\,\Delta\mathbf{e}^{\mathrm{T}}}{\|\,\Delta\mathbf{e}\,\|^2}\right] + \frac{b}{\|\,\Delta\mathbf{e}\,\|}\,\mathbb{I} \tag{A16}$$

We can show that the matrices in (A9) are

$$\begin{aligned}
\mathbb{A}_1 &= \mathbb{M}_1 + X_{0,n}\,\mathbb{M}_2 \\
\mathbb{A}_2 &= \tilde{k}(bs + aX_{0,n})\left[\frac{\Delta\mathbf{e}\,\mathbf{v}^{\mathrm{T}}}{\|\Delta\mathbf{e}\|}\right] \\
\mathbb{A}_3 &= \frac{2G}{R_n}\,\alpha X_{0,n}\left[\mathbb{I} + (a-1)\frac{\Delta\mathbf{e}\,\Delta\mathbf{e}^{\mathrm{T}}}{\|\Delta\mathbf{e}\|^2}\right] \\
\mathbb{A}_4 &= \frac{2G}{R_n} a X_{0,n}[\Delta\mathbf{e}\mathbf{v}^{\mathrm{T}}]
\end{aligned} \tag{A17}$$

while the row vectors in (A10) are

$$\begin{aligned}
\mathbf{b}_1 &= \mathbf{X}_n^{\mathrm{sT}}\mathbb{M}_2 + kbX_{0,n}\frac{\Delta\mathbf{e}^{\mathrm{T}}}{\|\Delta\mathbf{e}\|} \\
\mathbf{b}_2 &= \tilde{k}(as + bX_{0,n})\mathbf{v}^{\mathrm{T}} \\
\mathbf{b}_3 &= \frac{2G}{R_n}\,\alpha b X_{0,n}\,\frac{\Delta\mathbf{e}^{\mathrm{T}}}{\|\Delta\mathbf{e}\|} \\
\mathbf{b}_4 &= \frac{2G}{R_n}\,bX_{0,n}\|\Delta\mathbf{e}\|\mathbf{v}^{\mathrm{T}}
\end{aligned} \tag{A18}$$

where a column vector after a matrix, or a row vector before, represents a matrix–vector product as usual.

REFERENCES

1. Hong-Ki Hong, Chien-Shan Liu. Internal symmetry in bilinear elastoplasticity. *International Journal of Non-Linear Mechanics* 1999; **34**:279–288.
2. Auricchio F, Beirão da Veiga L. On a new integration scheme for von-mises plasticity with linear hardening. *International Journal for Numerical Methods in Engineering* 2003; **56**:1375–1396.
3. Chaboche JL. Constitutive equations for cyclic plasticity and cyclic visco-plasticity. *International Journal of Plasticity* 1989; **5**:247–302.
4. Lubliner J. *Plasticity Theory*. Macmillan: New York, 1990.
5. Simo JC, Hughes TJR. *Computational Inelasticity*. Springer: Berlin, 1998.
6. Simo JC. Topics on the numerical analysis and simulation of plasticity. In *Handbook of Numerical Analysis*, Ciarlet PG, Lions JL (eds), vol. III. Elsevier: Amsterdam, 1999.
7. Auricchio F, Taylor RL. Two material models for cyclic plasticity: nonlinear kinematic hardening and generalized plasticity. *International Journal of Plasticity* 1995; **11**:65–98.
8. Zienkiewicz OC, Taylor RL. *The Finite Element Method* (5th edn), vol. II. McGraw-Hill: New York, 2002.
9. Hong-Ki Hong, Chien-Shan Liu. Internal symmetry in the constitutive model of perfect elastoplasticity. *International Journal of Non-Linear Mechanics* 2000; **35**:447–466.
10. Chien-Shan Liu. Cone of non-linear dynamical system and group preserving schemes. *International Journal of Non-Linear Mechanics* 2001; **36**:1047–1068.
11. Auricchio F. Ce-driver. *Technical Report*, Dipartimento di Meccanica Strutturale—University of Pavia, 2001. Manual prepared for the European school of advanced studies of seismic risk reduction.
12. Taylor RL. A finite-element analysis program. *Technical Report*, University of California at Berkeley, 2000. http://www.ce.berkeley.edu/rlt

13. Krieg RD, Krieg DB. Accuracies of numerical solution methods for the elastic-perfectly plastic model. *Journal of Pressure Vessel Technology* (ASME) 1977; **99**:510–515.
14. Yoder PJ, Whirley RG. On the numerical implementation of elastoplastic models. *Journal of Applied Mechanics* 1984; **51**:283–288.
15. Montmitonnet P, Gratacos P, Chenot JL. An integration scheme for Prandtl–Reuss elastoplasic constitutive equations. *International Journal for Numerical Methods in Engineering* 1992; **33**:943–961.
16. Ristinmaa M, Tryding J. Exact integration of constitutive equations in elasto-plasticity. *International Journal for Numerical Methods in Engineering* 1993; **36**:2525–2544.
17. Wei Z, Peric D, Owen DRJ. Consistent linearization for the exact stress update of Prandtl–Reuss non-hardening elastoplastic models. *International Journal for Numerical Methods in Engineering* 1996; **39**: 1219–1235.
18. Diele F, Lopez L, Peluso R. The Cayley transform in the numerical solution of unitary differential systems. *Advances in Computational Mathematics* 1998; **8**:317–334.
19. Artioli E, Auricchio F, Beirão da Veiga L. Exponential-based integration algorithms for von-Mises plasticity with linear hardening. Part I: numerical tests on a novel 'optimal' scheme, submitted.
20. Artioli E, Auricchio F, Beirão da Veiga L. Exponential-based integration algorithms for von-Mises plasticity with linear hardening. Part II: consistency, accuracy and stability analysis, submitted.

